Analytical solution for two-dimensional magneto-thermo-mechanical response in FG hollow sphere

S. Mohammad Reza KHALILI[1,2]**, Amir Hossien MOHAZZAB**[1]**, Mohsen JABBARI**[1]

[1]*Islamic Azad University, South Tehran Branch, Faculty of Engineering,*
Department of Mechanical Engineering, Tehran-IRAN
e-mail:smrkhalili2005@gmail.com
[2]*Faculty of Engineering, Kingston University, London-UK*

Abstract

This paper presents the effect of the magnetic problem of a functionally graded (FG) hollow sphere subjected to mechanical and thermal loads. An analytical solution for stresses and perturbation of the magnetic field vector were determined using the direct method and the power series method. All of the material properties varied continuously across the thickness direction according to the power-law functions of radial directions. The aim of this work was to understand the effect of the magnetic field on a FG hollow sphere subjected to mechanical and thermal loads. The magnetic field decreased the radial displacement and circumferential stress due to mechanical load, and had a negligible effect on mechanical radial stress. The magnetic field also increased the radial displacement and the radial and circumferential stresses due to thermal load. Increasing the power-law indices of the functionally graded material (FGM) decreased all of the above quantities due to mechanical load.

Key Words: Magneto-thermo-mechanical, FG hollow sphere, magnetic field

Introduction

Functionally graded materials (FGMs) are heterogeneous and advanced materials in which the elastic and thermal properties vary gradually and continuously from one surface to another. FGMs decrease the thermal stresses and hence are very useful in nuclear, aircraft, and space engineering applications. The application of this issue is seen in geophysics, seismology, plasma physics, magnetic storage elements, magnetic structural elements, and measurement techniques of magneto-elasticity.

Chen and Lee (2003) worked on magneto-thermoelasticity by introducing 2 displacement and 2 stress functions. The governing equations of the linear theory of magneto-electro-thermoelasticity with transverse isotropy were simplified. The material nonhomogeneity along the axis of symmetry was taken into account and an approximate laminate model was employed to facilitate the deriving of analytical solutions. Dai and Fu (2007) recently considered the magneto-thermoelastic problem of FG hollow structures subjected to mechanical loads. The material stiffness, the thermal expansion coefficient, and the magnetic permeability were assumed to obey simple power-law variations through the structures' wall thickness. The aim of their research was to understand

the effect of composition on magneto-thermoelastic stresses and to design optimum FG hollow cylinders and hollow spheres. Dai and Wang (2006) presented an analytical method to solve the problem of the dynamic stress-focusing and centered-effect of perturbation of the magnetic field vector in orthotropic cylinders under thermal and mechanical shock loads. Analytical expressions for the dynamic stresses and the perturbation of the magnetic field vector were obtained by means of finite Hankel transforms and Laplace transforms. Recently, Poultangari et al. (2008) studied the nonaxisymmetric thermo-mechanical loads on functionally graded hollow spheres. Abd-Alla et al. (2004) presented an investigation of stress, temperature, and magnetic field in an isotropic, homogeneous, viscoelastic medium with a spherical cavity in a primary magnetic field, when the curved surface of the spherical cavity was subjected to periodic loading. Tianhu et al. (2004) reported the theory of generalized thermoelasticity, based on the theory of Lord and Shulman with one relaxation time, used to study the electro-magneto-thermoelastic interactions in a semi-infinite, perfectly conducting solid subjected to a thermal shock on its surface when the solid and its adjoining vacuum were subjected to a uniform axial magnetic field. They used Laplace transform in the analysis. Maxwell's equations were formulated and the generalized electro-magneto-thermoelastic coupled governing equations were established. Tianhu et al. (2005) reported a generalized electro-magneto-thermoelastic problem for an infinitely long solid cylinder based on the theory of Lord and Shulman with one relaxation time. Eslami et al. (2005) presented a general solution for one-dimensional, steady-state thermal and mechanical stresses in a hollow, thick sphere made of FGM. The material properties, except Poisson's ratio, were assumed to vary along the radius r according to a power-law function. Lee (2009) recently considered the problem of 3D, axisymmetric, quasistatic coupled magneto-thermoelasticity for laminated circular, conical shells subjected to magnetic and temperature fields. Laplace transform and finite difference methods were used to analyze the problem. He obtained solutions for the temperature and thermal deformation distributions in a transient and steady state. Lutz and Zimmerman (1996) solved the problem of the uniform heating of a spherical body whose elastic modulus and thermal expansion coefficient vary linearly with the radius. Maruszewski (1981) presented nonlinear magneto-thermoelastic equations in soft ferromagnetic and elastic bodies. The symmetry of couplings in these equations was also investigated. Massalas (1991) dealt with the phenomenological description of the magneto-thermoelastic interactions in a ferromagnetic material within the framework of the generalized theory of thermoelasticity proposed by Green and Laws. The material was assumed to be homogeneous, anisotropic, and elastic, undergoing large deformations. The analysis was based on the thermodynamic laws of quasi-magnetostatics. Misra et al. (1991) presented a solution for the induced temperature and stress fields in an infinite, transversely isotropic solid continuum with a cylindrical hole using the integral transform. The solid medium was considered to be exposed to a magnetic field and the cavity surface was assumed to be subjected to ramp-type heating. The Green and Lindsay model was used to account for the finite velocity of heat conduction. Misra et al. (1992) considered the problem of a half-space under the influence of an external primary magnetic field and an elevated temperature field arising out of the ramp-type heating of the surface. It was found that the stress distribution and the secondary magnetic field were almost independent of the thermal relaxation time, but were significantly dependent on the mechanical relaxation time. Paul and Narasimhan (1987) studied the problem of axisymmetric axial stress wave generation in a thermoelastic, circular cylindrical bar in the presence of an applied magnetic field. It was assumed that the surface of the cylinder was free from mechanical loadings and thermal radiation. A general solution was obtained by perturbation technique and was annihilated to a particular case, in which the applied magnetic field was constant in space and time. Sharma and Pal (2004) investigated the propagation of a magnetic-thermoelastic plane wave in an initially unstressed, homogeneous isotropic conducting plate under a uniform, static magnetic

field. The generalized theory of thermoelasticity was employed by assuming the electrical behavior as quasistatic and the mechanical behavior as dynamic. At short wavelength limits, the secular equations for symmetric and skew-symmetric modes were reduced to a Rayleigh surface wave frequency equation, because a finite-thickness plate in such situation behaves like a semi-infinite medium. Tanigawa et al. (1999) reported the derivation of systems of fundamental equations for a 3D thermoelastic field with nonhomogeneous material properties and its application to a semi-infinite body. Wang and Dong (2006) presented theoretical methods for analyzing magneto-thermoelastic responses and perturbation of the magnetic field vector in a conducting, nonhomogeneous, thermoelastic cylinder subjected to thermal shock. By making use of finite Hankel integral transforms, the analytical expressions were obtained for the magneto-thermodynamic stress and perturbation response of an axial magnetic field vector in a nonhomogeneous cylinder. Wang and Dink (2006) studied the transient responses of a magneto-electro-elastic hollow sphere for the fully coupled spherically symmetric problem. By means of the separation of variables technique and the electric and magnetic boundary conditions, the dynamic problem of a magneto-electro-elastic hollow sphere under spherically symmetric deformation was transformed to 2 Volterra integral equations of the second kind about 2 functions of time. Recently, Arani et al. (2009) developed an analytical response to the magneto-thermoelastic stress and perturbation of the magnetic field vector for a thick-walled, spherical FGM vessel placed in a uniform magnetic field. This vessel was subjected to an internal pressure and transient temperature gradient. The dynamic equation of magneto-thermoelasticity was solved using the Hankel and Laplace transform techniques. Loghman et al. (2010) recently presented a time-dependent creep stress redistribution analysis of a thick-walled FGM cylinder placed in uniform magnetic and temperature fields and subjected to internal pressure using the Prandtl-Reuss relation. The material creep and the magnetic and mechanical properties through the radial graded direction were assumed to obey the simple power-law variation. Yapıcı et al. (2010) studied the nonuniform temperature gradients and thermal stresses produced by a moving heat flux applied to a hollow sphere. Yapıcı and Baştürk (2006) studied the thermally induced stress in a solid disk heated by moving ring heat flux (radially periodic expanding and contracting) and subsequently cooled by means of a coolant following the heat flux. It was assumed that the ring heat flux per unit area at each ring surface was uniform. The Fluent 6.1 program was chosen as the computer code to calculate the numerical solutions, using the Simpson integration method. Yapıcı et al. (2008) studied the numerical analyses of transient temperature and thermally induced stress distributions in a stationary, hollow steel disk partially heated by a moving uniform heat source from its outer surface under stagnant ambient conditions. The moving heat source was applied on a certain angular segment of the processed surface, rotating with a constant angular speed. Özışık and Genç (2008) studied the temperature and thermal stress distribution in a plate heated from one side of its surface with a moving heat source. Genç et al. (2009) presented the effects of a moving heat source on a rotating hollow steel disk heated from one side of its surface under stagnant ambient conditions. As the disk rotated around the z-axis with a constant angular speed Ω, the heat source moved along from one radial segment to the next radial segment in the radial direction on the processed surface at the end of each revolution of the disk. Mahdi and Zhang (1997) investigated the correlation between the thermal residual stresses and conditions of surface grinding using a finite element. The effect of a coolant was simulated by heat convection. To obtain a reliable figure of thermal residual stresses induced by grinding, temperature-dependent properties of the work materials were taken into account and a nonuniform convection model with an effective cooling factor was introduced. Sen et al. (2000) studied the residual and thermal stresses that occur during water quenching of a solid cylindrical rod and ring cross-sectioned steel tubes, in which a finite element technique was used. The variations of residual stresses on different surfaces and cross-sections,

e.g. in the radial, axial, and tangential directions, were examined, and the effect of the internal diameter of the tubes on residual stress was investigated. Moulik et al. (2001) developed an efficient finite element procedure to calculate the temperatures and stresses arising due to a moving source of heat. The procedure was applied to calculate the thermal stresses produced in hardened steels during grinding.

In this work, the magnetic response of a FG hollow sphere subjected to mechanical and thermal loads was considered. Analytical solutions for stresses and perturbation of the magnetic field vector were determined using the infinitesimal theory of magneto-thermoelasticity. The material stiffness and the magnetic permeability varied continuously across the thickness direction according to power-law functions of radial direction. The results were validated with available results from the literature. The aim of this work was to understand the effect of magnetic field on a FG hollow sphere subjected to mechanical and thermal loads.

Heat conduction problem

Consider a hollow sphere of inner radius a and outer radius b, made of FGM. The spherical coordinates (r, θ, ϕ) are considered. The heat conduction equation for the 2D transient FG sphere is (Özışık, 1980):

$$T_{,rr} + (\frac{k'(r)}{k(r)} + \frac{2}{r})T_{,r} + \frac{1}{r^2}T_{,\theta\theta} + \frac{\cot\theta}{r^2}T_{,\theta} = 0$$

$$a \leq r \leq b, 0 \leq \theta \leq \pi \tag{1}$$

where k(r) is the heat conduction coefficient. The general thermal boundary conditions are considered to be:

$$\begin{cases} x_{11}T(a,\theta) + x_{12}T_{,r}(a,\theta) = F_1(\theta) \\ x_{21}T(b,\theta) + x_{22}T_{,r}(b,\theta) = F_2(\theta) \end{cases}. \tag{2}$$

By choosing suitable values for parameters $x_{ij}(i, j = 1, 2)$, different types of thermal boundary conditions, including conduction, heat flux, and convection, may be considered for the sphere. When a spherical vessel is not completely full of hot fluid, is under sun radiation on one side, or the temperatures of inlet and outlet nozzles are different, the distribution of temperature and stresses happens in a 2D and asymmetric form.

The material properties of the sphere are assumed to be graded along the thickness direction, according to the power-law function, as (Dai and Fu, 2007):

$$E(r) = E_0(\frac{r}{a})^{m_1}, \alpha(r) = \alpha_0(\frac{r}{a})^{m_2}, k(r) = k_0(\frac{r}{a})^{m_3}, \mu(r) = \mu_0(\frac{r}{a})^{m_4} \tag{3}$$

where $E_0, \alpha_0, k_0, \mu_0$ are respectively the modulus of elasticity, the thermal expansion coefficient, the heat conduction coefficient, and the magnetic permeability, and m_1, m_2, m_3, m_4 are the power-law indices. Since most of the literature deals with the power-law function, it was decided, for comparative purposes, to consider the power-law function for FGM. Meanwhile, the solutions obtained were simple in engineering problems. The solution for the temperature equation can be written in the form of a power series as:

$$T(r, \theta) = \sum_{n=0}^{+\infty} T_n(r)P_n(\cos\theta) \tag{4}$$

where $P_n(\cos\theta)$ is the Legendre series. Using the definition for material properties and Eq. (4), the heat conduction equation becomes:

$$T_n'' + (m_3 + 2)\frac{1}{r}T_n' - \frac{n(n+1)}{r^2}T_n = 0. \tag{5}$$

The solution for Eq. (5) is as follows:

$$T_n^g(r) = E_{1n}r^{\delta_{1n}} + E_{2n}r^{\delta_{2n}} \tag{6}$$

where

$$\delta_{1n,2n} = -\frac{m_3+1}{2} \pm \sqrt{\frac{(m_3+1)^2}{4} + n(n+1)}. \tag{7}$$

Therefore, by substituting Eq. (6) into Eq. (4), the solution of Eq. (5) is as follows:

$$T(r,\theta) = \sum_{n=0}^{+\infty}(E_{1n}r^{\delta_{1n}} + E_{2n}r^{\delta_{2n}})P_n(\cos\theta). \tag{8}$$

Constants E_{1n} and E_{2n} can be evaluated as follows by substituting Eq. (8) into the thermal boundary conditions:

$$E_{1n} = \frac{b^{\delta_{2n}}\frac{2n+1}{2}\int_0^\pi F_1(\theta)P_n(\cos\theta)\sin\theta d\theta - a^{\delta_{2n}}\frac{2n+1}{2}\int_0^\pi F_2(\theta)P_n(\cos\theta)\sin\theta d\theta}{a^{\delta_{1n}}b^{\delta_{2n}} - a^{\delta_{2n}}b^{\delta_{1n}}}$$

$$E_{2n} = \frac{a^{\delta_{1n}}\frac{2n+1}{2}\int_0^\pi F_2(\theta)P_n(\cos\theta)\sin\theta d\theta - b^{\delta_{1n}}\frac{2n+1}{2}\int_0^\pi F_1(\theta)P_n(\cos\theta)\sin\theta d\theta}{a^{\delta_{1n}}b^{\delta_{2n}} - a^{\delta_{2n}}b^{\delta_{1n}}}. \tag{9}$$

Stress Analysis

Let u and v be the displacement components in the radial and circumferential directions. Thus, the strain-displacement relations are:

$$\begin{aligned}
\varepsilon_{rr} &= u_{,r} \\
\varepsilon_{\theta\theta} &= \frac{1}{r}(u + v_{,\theta}) \\
\varepsilon_{\varphi\varphi} &= \frac{1}{r}(u + v\cot\theta) \\
\varepsilon_{r\theta} &= \frac{1}{2}\left(\frac{u_{,\theta}}{r} + v_{,r} - \frac{v}{r}\right)
\end{aligned} \tag{10}$$

Hooke's law for a 2D hollow sphere can be written as:

$$\sigma_{rr} = \frac{E(r)}{(1+\nu)(1-2\nu)}[(1-\nu)\varepsilon_{rr} + \nu\varepsilon_{\theta\theta} + \nu\varepsilon_{\varphi\varphi}] - \frac{E(r)\alpha(r)}{(1-2\nu)}T(r,\theta)$$

$$\sigma_{\theta\theta} = \frac{E(r)}{(1+\nu)(1-2\nu)}[\nu\varepsilon_{rr} + (1-\nu)\varepsilon_{\theta\theta} + \nu\varepsilon_{\varphi\varphi}] - \frac{E(r)\alpha(r)}{(1-2\nu)}T(r,\theta)$$

$$\sigma_{\varphi\varphi} = \frac{E(r)}{(1+\nu)(1-2\nu)}[\nu\varepsilon_{rr} + \nu\varepsilon_{\theta\theta} + (1-\nu)\varepsilon_{\varphi\varphi}] - \frac{E(r)\alpha(r)}{(1-2\nu)}T(r,\theta)$$

$$\sigma_{r\theta} = \frac{E(r)}{(1+\nu)}\varepsilon_{r\theta}. \tag{11}$$

The variation of the magnetic field with time or transient magnetic field results in an electrical field; when the magnetic field is uniform, there is no electrical field. When the electrical field vanishes, then the coefficient connecting the temperature gradient and the electrical current, as well as the coefficient connecting the current density and the heat flow density, like the Thompson effect, can be ignored. Assuming that the magnetic permeability, μ, of the FG hollow sphere is equal to the magnetic permeability of the medium around it, and that the medium is nonferromagnetic and nonferroelectric, and ignoring the Thompson effect, the simplified Maxwell's equations of electrodynamics for a perfectly conducting elastic medium are (Abd-Alla et al., 2004; Tianhu et al. 2004, 2005):

$$\vec{h} = \nabla \times (\vec{U} \times \vec{H}), \quad \vec{J} = \nabla \times \vec{h}, \quad f_i = \mu(r)(\vec{J} \times \vec{H})_i, \ (i = r, \theta). \tag{12}$$

The cubical dilatation is as follows:

$$e = \varepsilon_{rr} + \varepsilon_{\theta\theta} + \varepsilon_{\phi\phi} = u_{,r} + \frac{2}{r}u + \frac{1}{r}v_{,\theta} + \frac{1}{r}v\cot\theta. \tag{12.1}$$

Applying an initial magnetic field vector $\vec{H} = (0, 0, H_\phi)$ in spherical coordinates (r, θ, ϕ) to Eq. (9) yields:

$$\vec{U} = (u, v, 0), \quad \vec{h}_\phi = -H_\phi(e)$$

$$J = (-H_\phi \frac{1}{r}\frac{\partial e}{\partial \theta}, H_\phi \frac{\partial e}{\partial r}, 0), \ f = (H_\phi^2 \frac{\partial e}{\partial r}, H_\phi^2 \frac{1}{r}\frac{\partial e}{\partial \theta}, 0). \tag{13}$$

Thus, the Lorentz force is evaluated as follows:

$$f = \mu(r)H_\phi^2(u_{,rr} + \frac{2u_{,r}}{r} - \frac{2u}{r^2} + \frac{v_{,r\theta}}{r} - \frac{v_{,\theta}}{r^2} + \frac{\cot\theta v_{,r}}{r} - \frac{\cot\theta v}{r^2}, \frac{u_{,r\theta}}{r} + \frac{2u_{,\theta}}{r^2} + \frac{v_{,\theta\theta}}{r^2} + \frac{\cot\theta v_{,\theta}}{r^2} - \frac{(1+\cot^2\theta)v}{r^2}, 0). \tag{13.1}$$

The equilibrium equations of the FG hollow sphere, irrespective of the body force and the inertia terms, are:

$$\sigma_{rr,r} + \frac{1}{r}(\sigma_{r\theta,\theta} + 2\sigma_{rr} - \sigma_{\theta\theta} - \sigma_{\varphi\varphi} + \sigma_{r\theta}\cot\theta) + f_r = 0$$

$$\sigma_{r\theta,r} + \frac{1}{r}(\sigma_{\theta\theta,\theta} + (\sigma_{\theta\theta} - \sigma_{\varphi\varphi})\cot\theta + 3\sigma_{r\theta}) + f_\theta = 0 \tag{14}$$

Using Eqs. (10) through (14) and Eq. (3), the Navier equations in terms of radial and circumferential displacements are as follows:

$$u_{,rr} + (m_1 + 2)\frac{1}{r}u_{,r} + 2(\frac{m_1\nu}{1-\nu} - 1)\frac{1}{r^2}u + (\frac{1-2\nu}{2-2\nu})\frac{1}{r^2}u_{,\theta\theta} + (\frac{1-2\nu}{2-2\nu})\frac{\cot\theta}{r^2}u_{,\theta} + (\frac{1}{2-2\nu})\frac{1}{r}v_{,r\theta}$$

$$+ (\frac{m_1\nu}{1-\nu} - \frac{3-4\nu}{2-2\nu})\frac{1}{r^2}v_{,\theta} + (\frac{1}{2-2\nu})\frac{\cot\theta}{r}v_{,r} + (\frac{m_1\nu}{1-\nu} - \frac{3-4\nu}{2-2\nu})\frac{\cot\theta}{r^2}v$$

$$+ \frac{H_\phi^2\mu_0(1+\nu)(1-2\nu)}{E_0(1-\nu)}r^{m_4-m_1}(u_{,rr} + \frac{2}{r}u_{,r} - \frac{2}{r^2}u + \frac{1}{r}v_{,r\theta} - \frac{1}{r^2}v_{,\theta} + \frac{\cot\theta}{r}v_{,r} - \frac{\cot\theta}{r^2}v)$$

$$= \frac{(1+\nu)\alpha_0 a^{-m_2}}{1-\nu}[(m_1 + m_2)r^{m_2-1}T + r^{m_2}T_{,r}] \tag{15}$$

$$v_{,rr} + (m_1 + 2)\frac{1}{r}v_{,r} - (m_1 + (\frac{2-2\nu}{1-2\nu})(1+\cot^2\theta))\frac{1}{r^2}v + (\frac{2-2\nu}{1-2\nu})\frac{1}{r^2}v_{,\theta\theta} + (\frac{2-2\nu}{1-2\nu})\frac{\cot\theta}{r^2}v_{,\theta} + (\frac{1}{1-2\nu})\frac{1}{r}u_{,r\theta}$$

$$+ (m_1 + \frac{4-4\nu}{1-2\nu})\frac{1}{r^2}u_{,\theta} + \frac{2H_\phi^2\mu_0(1+\nu)}{E_0}r^{m_4-m_1}[\frac{1}{r}u_{,r\theta} + \frac{2}{r^2}u_{,\theta} + \frac{1}{r^2}v_{,\theta\theta} + \frac{\cot\theta}{r^2}v_{,\theta} - \frac{(1+\cot^2\theta)}{r^2}v]$$

$$= (\frac{2+2\nu}{1-2\nu})\alpha_0 a^{-m_2}r^{m_2-1}T_{,\theta}$$

For simplifying the Navier equations, it is assumed that the 2 power-law indices, m_1 and m_4, are equal. Therefore, the solutions of the Navier equations are:

$$u(r,\theta) = \sum_{n=0}^{+\infty} u_n(r) P_n(\cos\theta)$$
$$v(r,\theta) = \sum_{n=0}^{+\infty} v_n(r) \sin\theta P_n'(\cos\theta) \tag{16}$$

where $P_n(\cos\theta)$ is the Legendre series and $P_n'(\cos\theta)$ is the differentiation of the Legendre series with respect to the circumferential direction. Using Eq. (16) and substituting it into the Navier equations yields the following:

$$u_n''(1+A) + (m_1 + 2 + 2A)\frac{1}{r}u_n' + [2(\frac{\nu m_1}{1-\nu} - 1 - A) - n(n+1)(\frac{1-2\nu}{2-2\nu})]\frac{1}{r^2}u_n$$

$$+n(n+1)(\frac{1}{2-2\nu} + A)\frac{1}{r}v_n' + n(n+1)(\frac{\nu m_1}{1-\nu} - \frac{3-4\nu}{2-2\nu} - A)\frac{1}{r^2}v_n$$

$$= \frac{(1+\nu)\alpha_0 a^{-m_2}}{(1-\nu)}[(m_1 + m_2)r^{m_2-1}T_n + r^{m_2}T_n']$$

$$v_n'' + (m_1 + 2)\frac{1}{r}v_n' - [n(n+1)(\frac{2-2\nu}{1-2\nu}) + m_1 + Bn(n+1)]\frac{1}{r^2}v_n$$

$$-(\frac{1}{1-2\nu} + B)\frac{1}{r}u_n' - (m_1 + \frac{4-4\nu}{1-2\nu} + 2B)\frac{1}{r^2}u_n = -\frac{(2+2\nu)\alpha_0 a^{-m_2}}{(1-2\nu)}r^{m_2-1}T_n \tag{17}$$

where

$$A = \frac{H_\phi^2 \mu_0(1+\nu)(1-2\nu)}{E_0(1-\nu)}, B = \frac{2H_\phi^2 \mu_0(1+\nu)}{E_0}. \tag{18}$$

The symbol ($'$) denotes differentiation with respect to r. The general solutions of Eq. (17) are:

$$u_n^g(r) = Cr^\mu, v_n^g(r) = Dr^\mu. \tag{19}$$

Substituting Eq. (19) into the left side of Eq. (17) yields:

$$C\{\mu(\mu-1)(1+A) + (m+2+2A)\mu + \frac{2m\nu}{1-\nu} - 2 - 2A - n(n+1)(\frac{1-2\nu}{1-\nu})\} + \{n(n+1)(\frac{1}{2-2\nu} + A)\mu$$

$$+n(n+1)(\frac{m\nu}{1-\nu} - \frac{3-4\nu}{2-2\nu} - A)\}D = 0$$

$$D\{\mu(\mu-1) + (m+2)\mu - n(n+1)\frac{2-2\nu}{1-2\nu} - m - Bn(n+1)\} + C\{-\mu\,(\frac{1}{1-2\nu} + B) - (m + \frac{4-4\nu}{1-2\nu} + 2B)\} = 0. \tag{20}$$

Eq. (20) is a system of algebraic equations such that for obtaining their nontrivial solution, their determinant should be equal to 0, and their 4 roots are evaluated as follows:

$$\{\mu(\mu-1)(1+A) + (m+2+2A)\mu + \frac{2m\nu}{1-\nu} - 2 - 2A - n(n+1)(\frac{1-2\nu}{1-\nu})\} \times \{\mu(\mu-1) + (m+2)\mu$$

$$-n(n+1)(\frac{2-2\nu}{1-2\nu}) - m - Bn(n+1)\} + \{n(n+1)(\frac{1}{2-2\nu} + A)\mu +$$

$$n(n+1)(\frac{m\nu}{1-\nu} - \frac{3-4\nu}{2-2\nu} - A)\} \times \{\mu(\frac{1}{1-2\nu} + B) + m + \frac{4-4\nu}{1-2\nu} + 2B\} = 0 \tag{21}$$

Therefore,

$$u_n^g(r) = \sum_{j=1}^{4} C_{nj}r^{\mu_{nj}}, v_n^g(r) = \sum_{j=1}^{4} N_{nj}C_{nj}r^{\mu_{nj}} \tag{22}$$

where

$$N_{nj} = -\frac{\mu(\mu-1)(1+A) + (m+2+2A)\mu + \frac{2m\nu}{1-\nu} - 2 - 2A - n(n+1)(\frac{1-2\nu}{2-2\nu})}{n(n+1)[\mu(\frac{1}{2-2\nu}+A) + \frac{m\nu}{1-\nu} - \frac{3-4\nu}{2-2\nu} - A]} \quad j = (1,...,4) \; n \neq 0. \quad (23)$$

The particular solutions of Eq. (17) are assumed to be as follows:

$$\begin{aligned} u_n^p(r) &= F_{1n} r^{m_2+\delta_{1n}+1} + F_{2n} r^{m_2+\delta_{2n}+1} \\ v_n^p(r) &= F_{3n} r^{m_2+\delta_{1n}+1} + F_{4n} r^{m_2+\delta_{2n}+1} \end{aligned} \quad . \quad (24)$$

Substituting Eq. (24) into Eq. (17), the coefficients of the particular solution are evaluated from the algebraic system of equations solved by Cramer's method, as follows:

$$F_{1n} = \frac{d_5 d_4 - d_6 d_2}{d_1 d_4 - d_3 d_2}, F_{3n} = \frac{d_1 d_6 - d_3 d_5}{d_1 d_4 - d_3 d_2}$$

$$F_{2n} = \frac{d_{11} d_{10} - d_{12} d_8}{d_7 d_{10} - d_9 d_8}, F_{4n} = \frac{d_7 d_{12} - d_9 d_{11}}{d_7 d_{10} - d_9 d_8}. \quad (25)$$

The constants $d_1,\ldots,d_{12}$ are given in the Appendix. Combination of the decoupled case, for $n = 0$, must be considered:

$$u_{rr} - s_1 \frac{1}{r^2} u = s_2 r^{m_2-1} T + s_3 r^{m_2} T_r. \quad (26)$$

The general solution in this case is as follows:

$$u_0^g(r) = \sum_{i=1}^{2} a_{0i} r^{\eta_i} \quad (27)$$

$$\eta_{1,2} = \frac{1}{2} \pm \sqrt{\frac{1}{4} + \frac{(1-2\nu)(m_1+2+2A)(m_1+\frac{4-4\nu}{1-2\nu}+2B)}{(1+A)(1+B(1-2\nu))} - 2(\frac{m_1\nu}{(1+A)(1-\nu)} - 1)}. \quad (28)$$

The temperature distribution in this case becomes:

$$T_0(r) = E_{10} r^{\delta_{10}} + E_{20} r^{\delta_{20}} \quad (29)$$

where

$$\delta_{10,20} = 0, -m_3 - 1$$

$$E_{10} = \frac{b^{-m_3-1} \frac{1}{2} \int_0^\pi F_1(\theta) \sin\theta d\theta - a^{-m_3-1} \frac{1}{2} \int_0^\pi F_2(\theta) \sin\theta d\theta}{b^{-m_3-1} - a^{-m_3-1}} \quad (30)$$

$$E_{20} = \frac{\frac{1}{2} \int_0^\pi F_2(\theta) \sin\theta d\theta - \frac{1}{2} \int_0^\pi F_1(\theta) \sin\theta d\theta}{b^{-m_3-1} - a^{-m_3-1}}$$

and the particular solution for displacement of the decoupled case is:

$$u_0^p(r) = F_{10} r^{m_2-m_3} + F_{20} r^{m_2+1} \quad (31)$$

where

$$F_{10} = \frac{[s_2 - s_3(m_3 + 1)]E_{20}}{(m_2 - m_3)(m_2 - m_3 - 1) - s_1} \tag{32}$$

$$F_{20} = \frac{s_2 E_{10}}{(m_2 + 1)m_2 - s_1}.$$

Therefore, the solution of the Navier equations for the 2D hollow sphere is obtained as follows:

$$
\begin{aligned}
u(r,\theta) &= \sum_{n=1}^{+\infty}\{\sum_{j=1}^{4} C_{nj}r^{\mu_{nj}} + F_{1n}r^{m_2+\delta_{1n}+1} + F_{2n}r^{m_2+\delta_{2n}+1}\}P_n(\cos\theta) + \sum_{i=1}^{2} a_{0i}r^{\eta_i} + F_{10}r^{m_2-m_3} + F_{20}r^{m_2+1} \\
v(r,\theta) &= \sum_{n=1}^{+\infty}\{\sum_{j=1}^{4} N_{nj}C_{nj}r^{\mu_{nj}} + F_{3n}r^{m_2+\delta_{1n}+1} + F_{4n}r^{m_2+\delta_{2n}+1}\}\sin\theta P_n'(\cos\theta)
\end{aligned}
$$

.

$$\tag{33}$$

Substituting Eq. (33) in Eq. (10) yields:

$$
\begin{aligned}
\varepsilon_{rr} &= \sum_{n=1}^{+\infty}\{\sum_{j=1}^{4} \mu_{nj}C_{nj}r^{\mu_{nj}-1} + (m_2+\delta_{1n}+1)F_{1n}r^{m_2+\delta_{1n}} + (m_2+\delta_{2n}+1)F_{2n}r^{m_2+\delta_{2n}}\}P_n(\cos\theta) \\
&\quad + \sum_{i=1}^{2}\eta_i a_{0i}r^{\eta_i-1} + (m_2-m_3)F_{10}r^{m_2-m_3-1} + (m_2+1)F_{20}r^{m_2}
\end{aligned}
$$

$$
\begin{aligned}
\varepsilon_{\theta\theta} &= \sum_{n=1}^{+\infty}\{\sum_{j=1}^{4} C_{nj}r^{\mu_{nj}-1} + F_{1n}r^{m_2+\delta_{1n}} + F_{2n}r^{m_2+\delta_{2n}}\}P_n(\cos\theta) + \sum_{i=1}^{2} a_{0i}r^{\eta_i-1} + F_{10}r^{m_2-m_3-1} + F_{20}r^{m_2} \\
&\quad + \sum_{n=1}^{+\infty}\{\sum_{j=1}^{4} N_{nj}C_{nj}r^{\mu_{nj}-1} + F_{3n}r^{m_2+\delta_{1n}} + F_{4n}r^{m_2+\delta_{2n}}\}[n(n+1)P_n(\cos\theta) - \cos\theta P_n'(\cos\theta)]
\end{aligned}
$$

$$
\begin{aligned}
\varepsilon_{\varphi\varphi} &= \sum_{n=1}^{+\infty}\{\sum_{j=1}^{4} C_{nj}r^{\mu_{nj}-1} + F_{1n}r^{m_2+\delta_{1n}} + F_{2n}r^{m_2+\delta_{2n}}\}P_n(\cos\theta) + \sum_{i=1}^{2} a_{0i}r^{\eta_i-1} \\
&\quad + F_{10}r^{m_2-m_3-1} + F_{20}r^{m_2} + \sum_{n=1}^{+\infty}\{\sum_{j=1}^{4} N_{nj}C_{nj}r^{\mu_{nj}-1} + F_{3n}r^{m_2+\delta_{1n}} + F_{4n}r^{m_2+\delta_{2n}}\}\cos\theta P_n'(\cos\theta)
\end{aligned}
$$

$$
\begin{aligned}
\varepsilon_{r\theta} &= \tfrac{1}{2}\{-\sum_{n=1}^{+\infty}\{\sum_{j=1}^{4} C_{nj}r^{\mu_{nj}-1} + F_{1n}r^{m_2+\delta_{1n}} + F_{2n}r^{m_2+\delta_{2n}}\} + \sum_{j=1}^{4}(\mu_{nj}-1)N_{nj}C_{nj}r^{\mu_{nj}-1} \\
&\quad + (m_2+\delta_{1n})F_{3n}r^{m_2+\delta_{1n}} + (m_2+\delta_{2n})F_{4n}r^{m_2+\delta_{2n}}\}\sin\theta P_n'(\cos\theta)\}
\end{aligned}
$$

.

$$\tag{34}$$

Substituting Eq. (34) into Eq. (11), the stress components are obtained as follows:

$$
\begin{aligned}
\sigma_{rr} &= \frac{E(r)}{(1+\nu)(1-2\nu)}\{(1-\nu)\sum_{n=1}^{+\infty}\{\sum_{j=1}^{4} \mu_{nj}C_{nj}r^{\mu_{nj}-1} + (m_2+\delta_{1n}+1)F_{1n}r^{m_2+\delta_{1n}} \\
&\quad + (m_2+\delta_{2n}+1)F_{2n}r^{m_2+\delta_{2n}}\}P_n(\cos\theta) + \sum_{i=1}^{2}\eta_i a_{0i}r^{\eta_i-1} + (m_2-m_3)F_{10}r^{m_2-m_3-1} \\
&\quad + (m_2+1)F_{20}r^{m_2} + \nu[2\sum_{n=1}^{+\infty}\{\sum_{j=1}^{4} C_{nj}r^{\mu_{nj}-1} + F_{1n}r^{m_2+\delta_{1n}} + F_{2n}r^{m_2+\delta_{2n}}\}P_n(\cos\theta)
\end{aligned}
$$

$$+2\sum_{i=1}^{2} a_{0i}r^{\eta_i-1} + 2F_{10}r^{m_2-m_3-1} + 2F_{20}r^{m_2}$$

$$+n(n+1)\sum_{n=1}^{+\infty}\{\sum_{j=1}^{4} N_{nj}C_{nj}r^{\mu_{nj}-1} + F_{3n}r^{m_2+\delta_{1n}} + F_{4n}r^{m_2+\delta_{2n}}\}P_n(\cos\theta)\}$$

$$\sigma_{\theta\theta} = \frac{E(r)}{(1+\nu)(1-2\nu)}\{\nu[\sum_{n=1}^{+\infty}\{\sum_{j=1}^{4}(\mu_{nj}+1)C_{nj}r^{\mu_{nj}-1} + (m_2+\delta_{1n}+2)F_{1n}r^{m_2+\delta_{1n}}$$

$$+(m_2+\delta_{2n}+2)F_{2n}r^{m_2+\delta_{2n}}\}P_n(\cos\theta) + \sum_{i=1}^{2}(\eta_i+1)a_{0i}r^{\eta_i-1}$$

$$+(m_2-m_3+1)F_{10}r^{m_2-m_3-1} + (m_2+2)F_{20}r^{m_2}$$

$$+\sum_{n=1}^{+\infty}\{\sum_{j=1}^{4} N_{nj}C_{nj}r^{\mu_{nj}-1} + F_{3n}r^{m_2+\delta_{1n}} + F_{4n}r^{m_2+\delta_{2n}}\}\cos\theta P_n'(\cos\theta)]$$

$$+(1-\nu)[\sum_{n=1}^{+\infty}\{\sum_{j=1}^{4}C_{nj}r^{\mu_{nj}-1} + F_{1n}r^{m_2+\delta_{1n}} + F_{2n}r^{m_2+\delta_{2n}}\}P_n(\cos\theta) + \sum_{i=1}^{2}a_{0i}r^{\eta_i-1}$$

$$+F_{10}r^{m_2-m_3-1} + F_{20}r^{m_2} + \sum_{n=1}^{+\infty}\{\sum_{j=1}^{4} N_{nj}C_{nj}r^{\mu_{nj}-1} + F_{3n}r^{m_2+\delta_{1n}} + F_{4n}r^{m_2+\delta_{2n}}\}$$

$$\times[n(n+1)P_n(\cos\theta) - \cos\theta P_n'(\cos\theta)]\}$$

$$\sigma_{\phi\phi} = \frac{E(r)}{(1+\nu)(1-2\nu)}\{\nu[\sum_{n=1}^{+\infty}\{\sum_{j=1}^{4}(\mu_{nj}+1)C_{nj}r^{\mu_{nj}-1} + (m_2+\delta_{1n}+2)F_{1n}r^{m_2+\delta_{1n}}$$

$$+(m_2+\delta_{2n}+2)F_{2n}r^{m_2+\delta_{2n}}\}P_n(\cos\theta) + \sum_{i=1}^{2}(\eta_i+1)a_{0i}r^{\eta_i-1}$$

$$+(m_2-m_3+1)F_{10}r^{m_2-m_3-1} + (m_2+2)F_{20}r^{m_2}$$

$$+\sum_{n=1}^{+\infty}\{\sum_{j=1}^{4} N_{nj}C_{nj}r^{\mu_{nj}-1} + F_{3n}r^{m_2+\delta_{1n}} + F_{4n}r^{m_2+\delta_{2n}}\}$$

$$\times(n(n+1)P_n(\cos\theta) - \cos\theta P_n'(\cos\theta))] + (1-\nu)[\sum_{n=1}^{+\infty}\{\sum_{j=1}^{4}C_{nj}r^{\mu_{nj}-1}$$

$$+F_{1n}r^{m_2+\delta_{1n}} + F_{2n}r^{m_2+\delta_{2n}}\}P_n(\cos\theta) + \sum_{i=1}^{2}a_{0i}r^{\eta_i-1} + F_{10}r^{m_2-m_3-1} + F_{20}r^{m_2}$$

$$+\sum_{n=1}^{+\infty}\{\sum_{j=1}^{4} N_{nj}C_{nj}r^{\mu_{nj}-1} + F_{3n}r^{m_2+\delta_{1n}} + F_{4n}r^{m_2+\delta_{2n}}\}\cos\theta P_n'(\cos\theta)]\}$$

$$\sigma_{r\theta} = \frac{E(r)}{2(1+\nu)}\{-\sum_{n=1}^{+\infty}\{\sum_{j=1}^{4}C_{nj}r^{\mu_{nj}-1} + F_{1n}r^{m_2+\delta_{1n}} + F_{2n}r^{m_2+\delta_{2n}}\} + \sum_{j=1}^{4}(\mu_{nj}-1)N_{nj}C_{nj}r^{\mu_{nj}-1}$$

$$+(m_2+\delta_{1n})F_{3n}r^{m_2+\delta_{1n}} + (m_2+\delta_{2n})F_{4n}r^{m_2+\delta_{2n}}\}\sin\theta P_n'(\cos\theta)\}. \tag{35}$$

Substituting Eq. (34) into Eq. (13), the perturbation of the magnetic field vector is:

$$h_\phi = -H_\phi \times \{\sum_{n=1}^{+\infty}\{\sum_{j=1}^{4}(\mu_{nj}+2)C_{nj}r^{\mu_{nj}-1} + (m_2+\delta_{1n}+3)F_{1n}r^{m_2+\delta_{1n}} + (m_2+\delta_{2n}+3)F_{2n}r^{m_2+\delta_{2n}}\}$$

$$+n(n+1)\sum_{j=1}^{4}N_{nj}C_{nj}r^{\mu_{nj}-1}+F_{3n}r^{m_2+\delta_{1n}} + F_{4n}r^{m_2+\delta_{2n}}\}P_n(\cos\theta) + \sum_{i=1}^{2}(\eta_i+2)a_{0i}r^{\eta_i-1} \tag{36}$$

$$+(m_2-m_3+2)F_{10}r^{m_2-m_3-1} + (m_2+3)F_{20}r^{m_2}\}.$$

The von Mises stress is as follows:

$$\sigma_v = \sqrt{(\sigma_{rr}-\sigma_{\theta\theta})^2 + (\sigma_{\theta\theta}-\sigma_{\phi\phi})^2 + (\sigma_{\phi\phi}-\sigma_{rr})^2 + 6\sigma_{r\theta}^2}\Big/\sqrt{2}. \tag{37}$$

To determine the displacements and stresses, 4 boundary conditions are required to evaluate the 4 unknown constants, C_{n1} to C_{n4} and a_{01}, a_{02}. The 4 boundary conditions may be selected from the list of boundary conditions given in Eq. (38). The procedure is continued by expanding the given boundary conditions into the Legendre series. These constants are calculated by solving the system of algebraic equations formed by 4 boundary conditions in the following expressions:

$$\begin{aligned} u(a,\theta) = g_1(\theta), u(b,\theta) = g_2(\theta) \qquad &\sigma_{rr}(a,\theta) = g_5(\theta), \sigma_{rr}(b,\theta) = g_6(\theta) \\ v(a,\theta) = g_3(\theta), v(b,\theta) = g_4(\theta). \qquad &\sigma_{r\theta}(a,\theta) = g_7(\theta), \sigma_{r\theta}(b,\theta) = g_8(\theta) \end{aligned} \tag{38}$$

where $g_i(\theta), (i = 1, ..., 8)$ are known boundary condition functions.

Results and Discussion

The present analytical solution may be validated by the results of previously published work. A simpler example of this work is presented in Eslami et al. (2005), in which the FG sphere was subjected to only mechanical load. The material properties and boundary conditions were assumed to be the same as in Eslami et al. (2005). The FG sphere was fixed at the outer surface ($U(b,\theta) = 0, V(b,\theta) = 0$) and subjected to mechanical stress at the inner surface of the sphere as: $\sigma_{rr}(a,\theta) = 400\cos 4\theta$, $\sigma_{r\theta}(a,\theta) = 0$. Figures 1 and 2 show, respectively, the radial displacement and the stress due to mechanical load obtained from the present analysis. These results are identical to those reported in Eslami et al. (2005), which indicates good agreement with previous publications. Figure 3 shows the temperature distribution under the thermal conditions of Eslami et al. (2005), Table, as $T(a,\theta) = 50\cos\theta^2/2$ and zero temperature at the outer radius, and the mechanical boundary conditions were fixed at the inner radius and traction-free at the outer radius. This figure is the same as Figure 6 in Eslami et al. (2005).
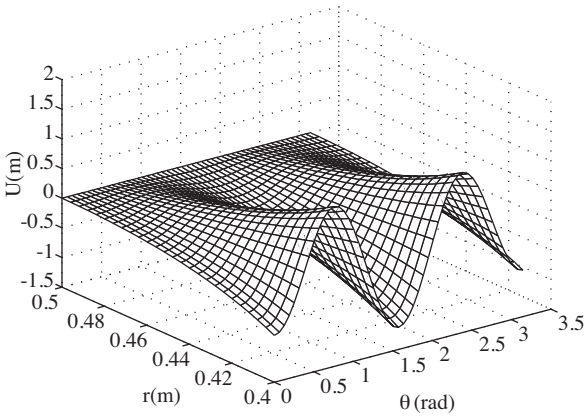
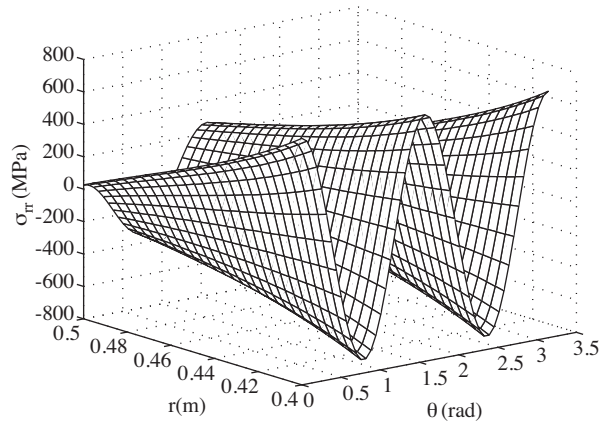**Figure 1.** Radial displacement due to mechanical load without magnetic field.

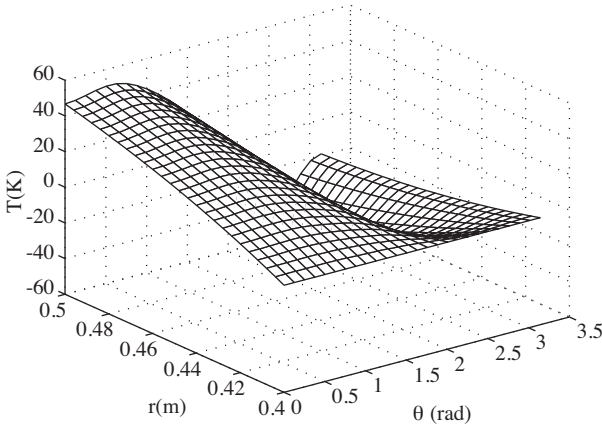**Figure 2.** Radial stress due to mechanical load without magnetic field.

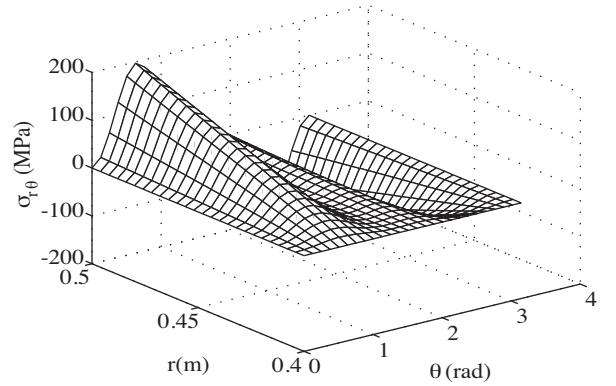**Figure 3.** Temperature distribution at $m = 1$.

Figure 4. Shear stress due to mechanical load and magnetic field (example 1).

As the first example, the effect of the magneto-mechanical response of an FG hollow sphere of inner radius (metal constituent) $a = 0.4$ m and outer radius (ceramic constituent) $b = 0.5$ m was considered. Poisson's ratio was assumed to be constant and was taken as 0.3, $H_\phi = 2.23 \times 10^9 (A/m)$, and $\mu_0 = 4\pi \times 10^{-7} (H/m)$ (Dai and Fu, 2007). The evaluated power-law indices and material properties used for the analysis are given in the Table.

In this section, the magneto-elastic and magneto-thermoelastic stresses were considered separately, because the values and order of magnitudes of these stresses were not the same, and surveying each of them clearly would be impossible.

The mechanical boundary conditions were assumed to be as follows:

$$\sigma_{rr}(a, \theta) = 0, \sigma_{rr}(b, \theta) = 400 \cos(3\theta)$$
$$\sigma_{r\theta}(a, \theta) = 0, \sigma_{r\theta}(b, \theta) = 200 \sin(3\theta) \quad .$$

Figure 4 shows the shear stress due to mechanical load and magnetic field. The shear stress is 0 on the internal surface, because in this example, this surface is considered to be traction-free. This Figure obeys

harmonic patterns. Figures 5-7 show the effect of the magnetic field on radial displacement, radial stress, and circumferential stress of the FG hollow sphere in the presence of a mechanical load for the evaluated power-law indices indicated in the Table and at various θ. The left-side figures correspond to the effect without a magnetic field, and the right-side figures correspond to the effect with a magnetic field. It is to be noted that the radial displacement due to mechanical load with a magnetic field is smaller in magnitude than the radial displacement due to mechanical load without a magnetic field. Radial stress due to mechanical load with a magnetic field is almost similar in magnitude and variation to the radial stress due to mechanical load without a magnetic field. At both the inner and outer surfaces, the radial stresses are equal in magnitude. Circumferential stress due to mechanical load without a magnetic field is greater in magnitude than the circumferential stress due to mechanical load with a magnetic field. The variations of the curves with and without a magnetic field are almost similar through the wall thickness.
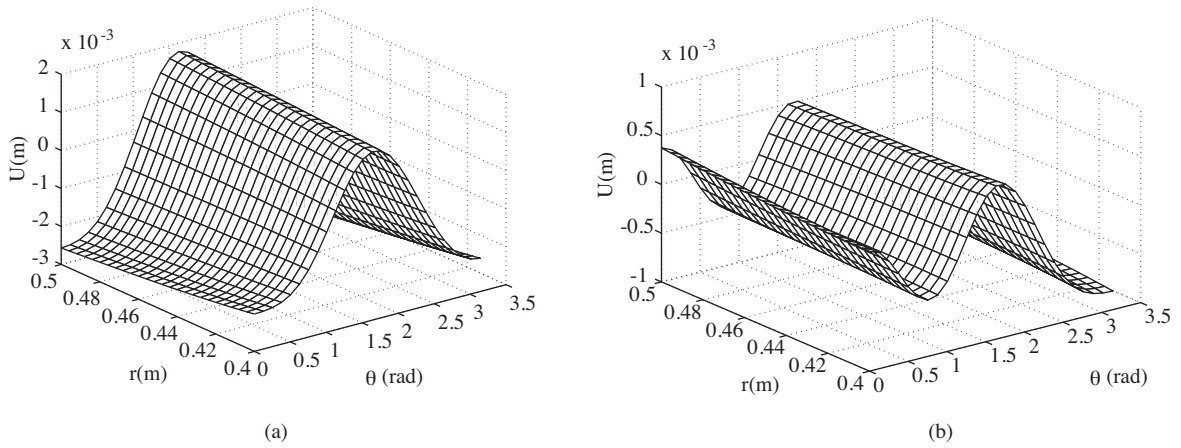
Figure 5. Radial displacement due to mechanical load a) without magnetic field and b) with magnetic field.
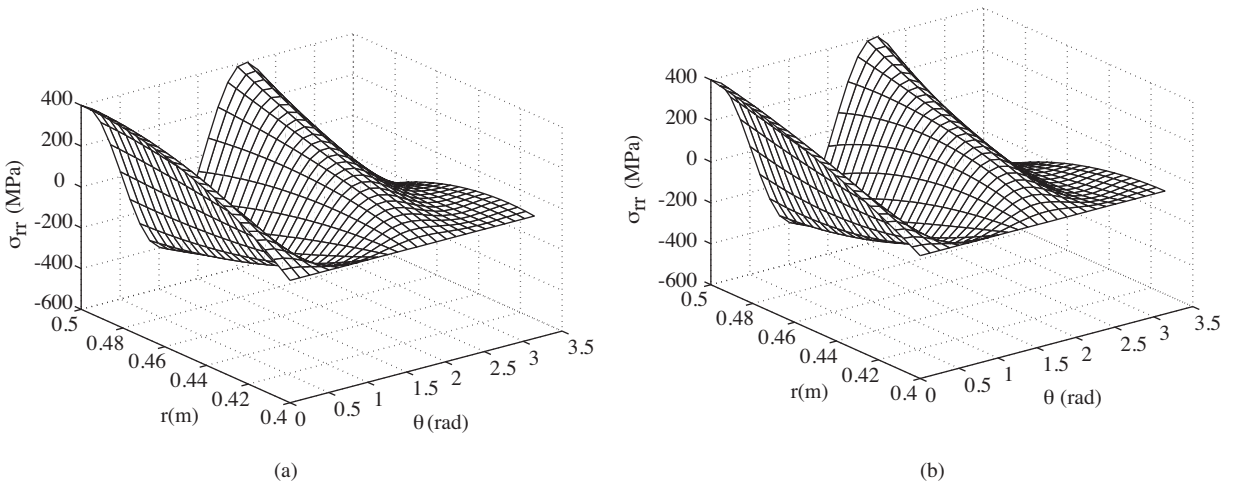

Figure 6. Radial stress due to mechanical load a) without magnetic field and b) with magnetic field.

In order to study the effect of power-law indices on the behavior of the first example of the FG hollow sphere in the Table in the presence of a magnetic field and mechanical load, the power indices of material properties were considered to be identical, $m_1 = m_2 = m_3 = m$. For this case, m was considered to range from -2 to +2. The zero-value of m corresponds to pure material. The positive value of m states the increase of the
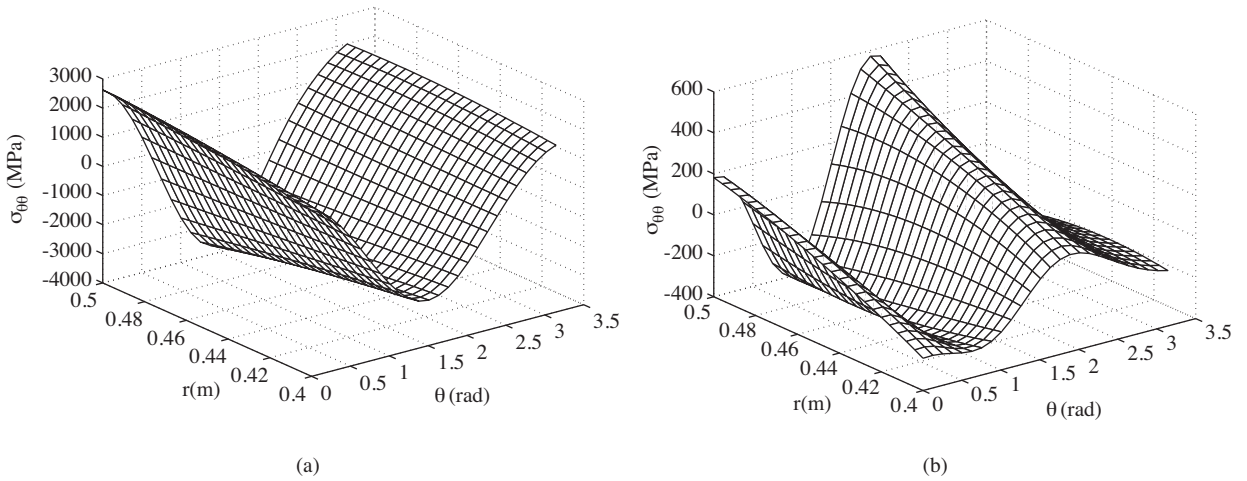
243

Figure 7. Circumferential stress due to mechanical load a) without magnetic field and b) with magnetic field.

Table. Material properties and evaluated power-law indices for the examples in the present study.

Power-law indices		Ceramic	Metal
Second example $a = 1.0$ m, $b = 1.2$ m	First example $a = 0.4$ m, $b = 0.5$ m		
$m_1 = m_4 = 3.1236$	$m_1 = m_4 = 2.5521$	$E = 117 GPa$	$E = 66.2 GPa$
$m_2 = -2.0329$	$m_2 = -1.6610$	$\alpha = 7.11 \times 10^{-6}\,{}^\circ K$	$\alpha = 10.3 \times 10^{-6}\,{}^\circ K$
$m_3 = -11.9839$	$m_3 = 9.7916$	$k = 2.036\,W/m\,{}^\circ K$	$k = 18.1\,W/m\,{}^\circ K$

ceramic constituent in the FGM and the negative value of m states the increase of the metal constituent in the FGM. Figures 8-11 show the distributions of radial displacement, radial stress, and circumferential and shear stresses due to mechanical load and magnetic field for various FGM power-law indices. Figure 12 shows the perturbation of the magnetic field vector due to mechanical load with power-law indices. As can be seen, when the power-law index (m) increased, the radial displacement, the radial, circumferential, and shear stresses due to mechanical load and magnetic field, and the perturbation of the magnetic field vector due to mechanical load all decreased. The variation of displacement is uniform through the wall thickness for all values of m considered here. The radial and shear stresses at both the inner and outer radius of the sphere are identical for different values of m; that is, for the above boundary conditions at the inner and outer radius of the sphere, m does not affect the radial or shear stresses. However, its contribution to changing the circumferential stresses at these surfaces is high; that is, at the inner surface of the sphere, by changing the value of m from -2 to +2, the circumferential stresses are changed by 60%, and at the outer surface of the sphere, the effect of changing m is almost negligible. Figure 13 shows the mechanical von Mises stress due to the magnetic field vector. As can be seen, with increasing power-law indices, the maximum of the von Mises stress from inside the sphere turns to the mid-radius of the sphere. This graph has a minimum value near the outside sphere at $r = 0.8$ thickness, and at this point, all of the von Mises stresses with different power-law indices are almost equal. Figure 14 shows the mechanical von Mises stress, without a magnetic field vector, for $m = 1$. The effective stress remained almost constant and the hollow sphere became optimum.

The second example consisted of considering the magneto-thermoelasticity response in a FG hollow sphere with inner radius (metal constituent) $a = 1$ m and outer radius (ceramic constituent) $b = 1.2$ m, with the same material properties as in the first example. The evaluated power-law indices for the second example
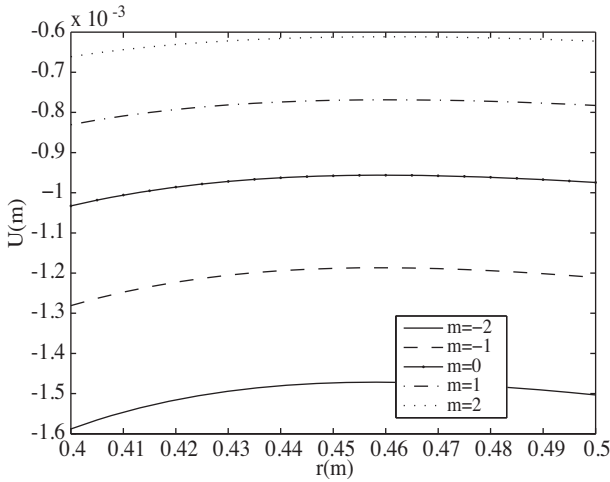
Figure 8. Radial displacement due to mechanical load and magnetic field along the thickness of the FG sphere with various power-law indices at $\theta = \pi/3$ (example 1).
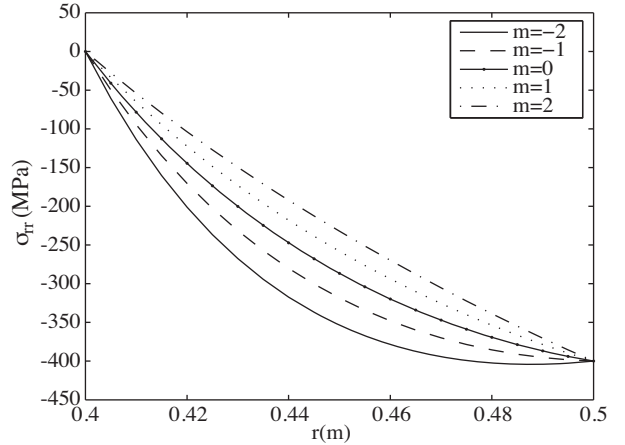

Figure 9. Radial stress due to mechanical load and magnetic field along the thickness of the FG sphere with various power-law indices at $\theta = \pi/3$ (example 1).
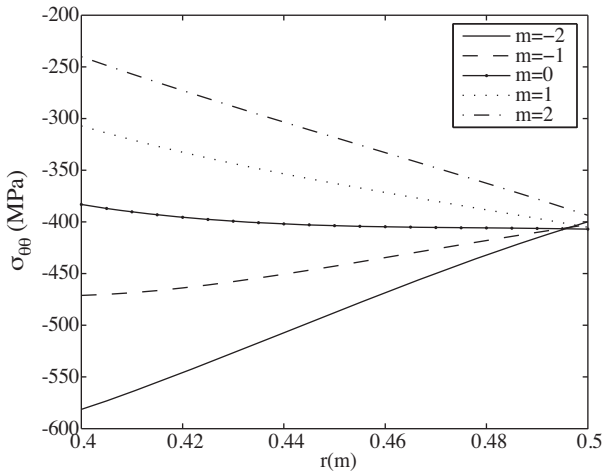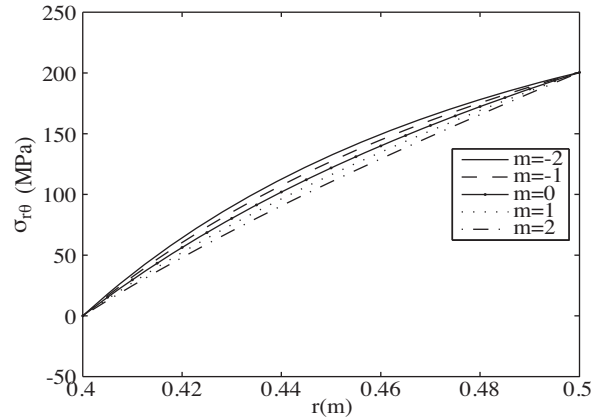

Figure 10. Circumferential stress due to mechanical load and magnetic field along the thickness of the FG sphere with various power-law indices at $\theta = \pi/3$ (example 1).

Figure 11. Shear stress due to mechanical load and magnetic field along the thickness of the FG sphere with various power-law indices at $\theta = \pi/3$ (example 1).

are given in the Table. The temperature at the inner radius is 0, and that at the outer radius is defined by $T(b, \theta) = 100 \cos \theta^2 / 2$. The mechanical boundary conditions are considered to be traction-free on both sides of the sphere. Figures 15-17 show, respectively, the effect of the magnetic field on radial displacement, radial stress, and circumferential stress of the FG hollow sphere, considering the thermal load as defined above and for the evaluated power-law indices indicated in the Table and at various θ. The left-side figures correspond to the effect without a magnetic field and the right-side figures correspond to the effect with a magnetic field. It is to be noted that the radial displacement due to thermal load with a magnetic field is greater in magnitude than the radial displacement due to thermal load without a magnetic field. The variations of both cases of displacement are almost the same. The radial stress due to thermal load without a magnetic field is smaller in magnitude

than the radial stress due to thermal load with a magnetic field. The variations of the 2 cases are completely different. At both the inner and outer surfaces, the radial stresses are equal in magnitude. Circumferential stress due to thermal load with a magnetic field is greater in magnitude than the circumferential stress due to thermal load without a magnetic field. The variations of the curves for the sphere subjected to a magnetic field and without a magnetic field are almost the same.
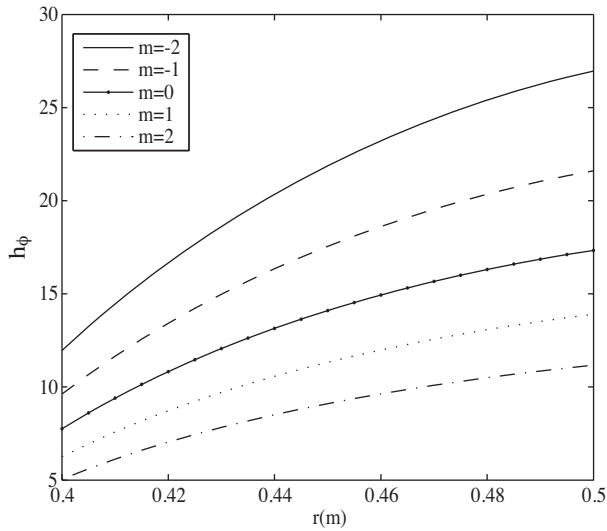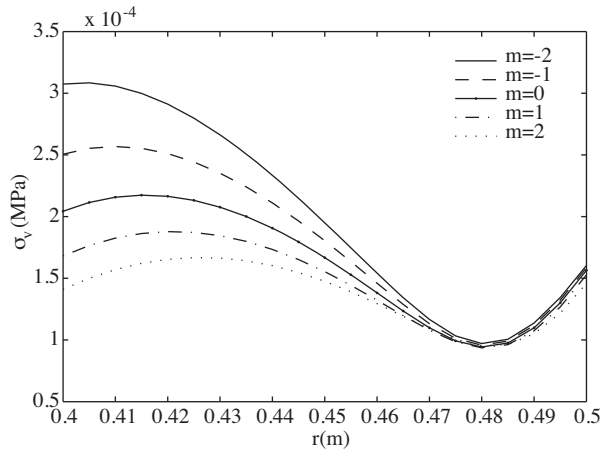

Figure 12. Perturbation of the magnetic field vector due to mechanical load along the thickness of the FG sphere with various power-law indices at $\theta = \pi/3$ (example 1).

Figure 13. Mechanical von Mises stress due to magnetic field vector along the thickness of the FG sphere with various power-law indices at $\theta = \pi/3$ (example 1).
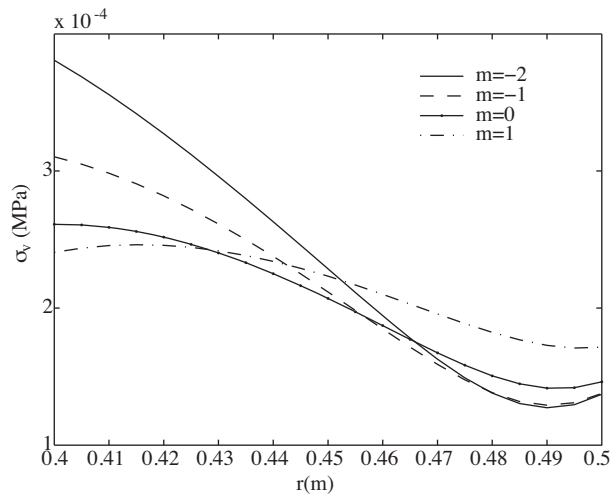

Figure 14. Mechanical von Mises stress without magnetic field vector along the thickness of the FG sphere with various power-law indices at $\theta = \pi/3$ (example 1).
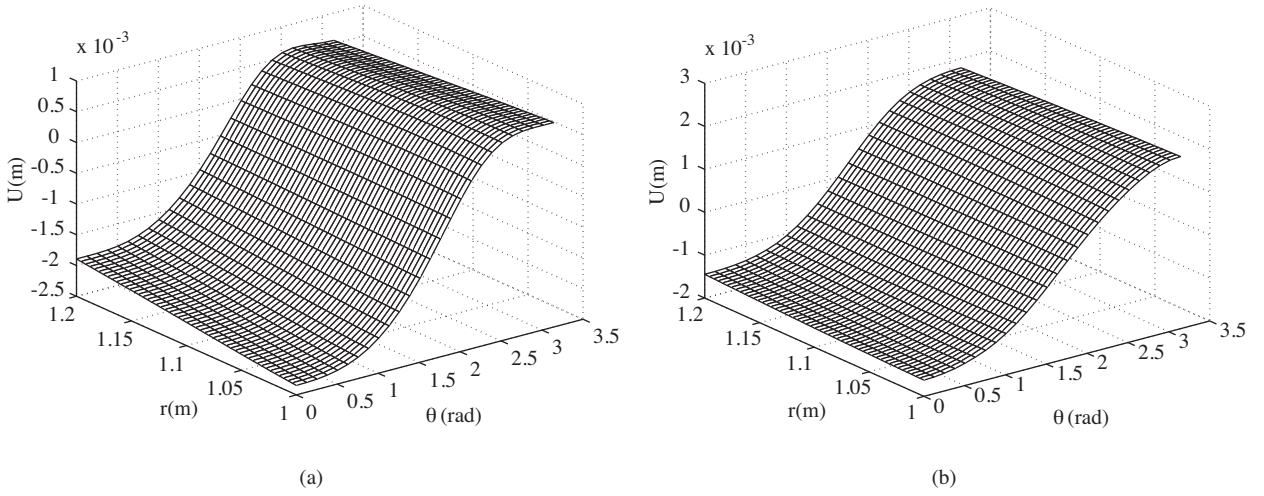
246

(a)

(b)

Figure 15. Radial displacement due to thermal load a) without magnetic field and b) with magnetic field.
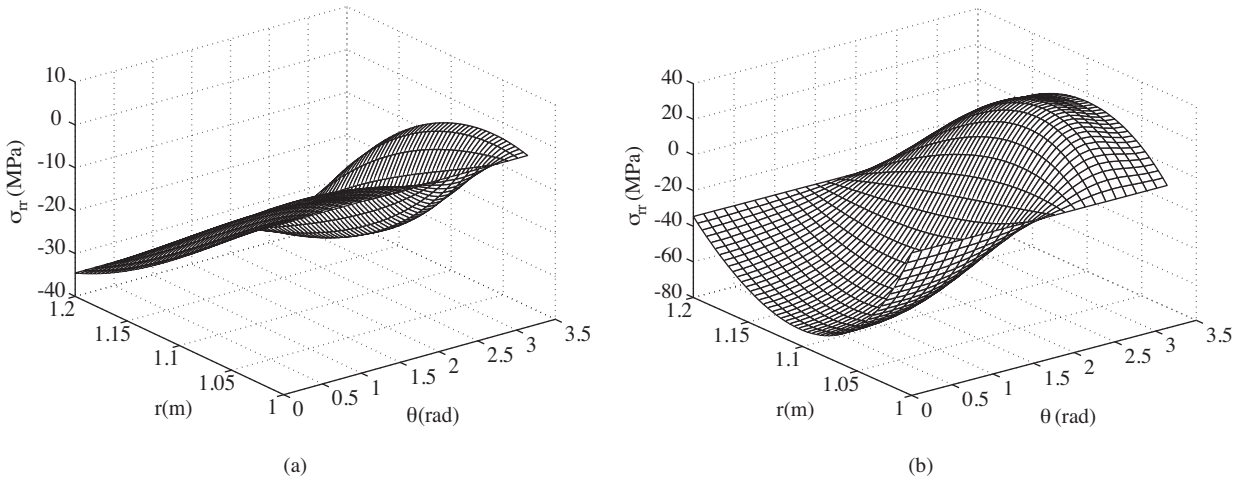

(a)

(b)

Figure 16. Radial stress due to thermal load a) without magnetic field and b) with magnetic field.
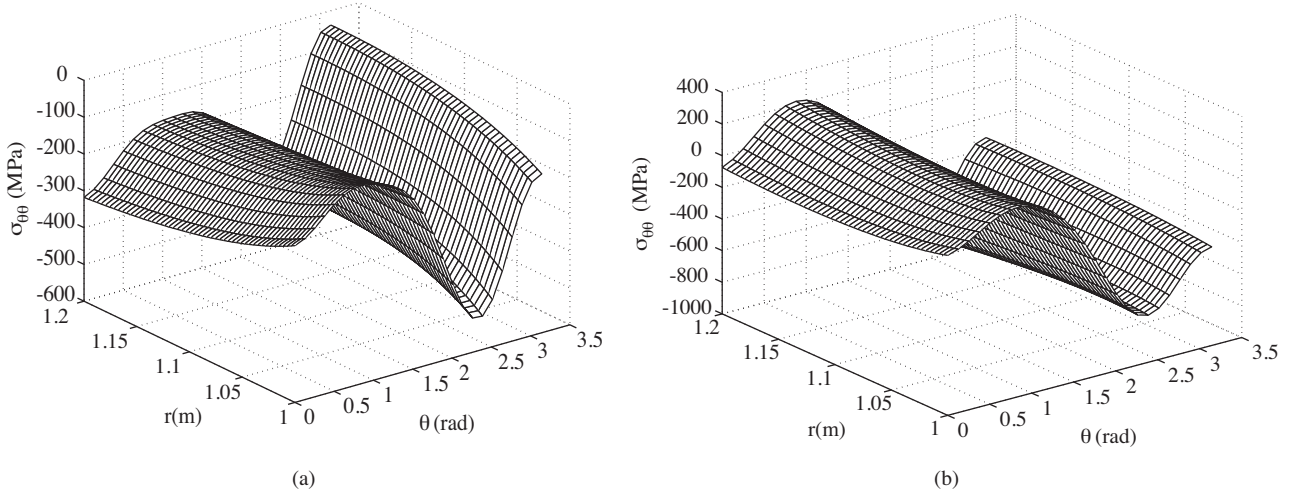

(a)

(b)

Figure 17. Circumferential stress due to thermal load a) without magnetic field and b) with magnetic field.

247

In order to study the effect of power-law indices on the behavior of the second example of the FG hollow sphere in the Table in the presence of a magnetic field and thermal load, the power indices of the material properties were considered to be identical, $m_1 = m_2 = m_3 = m$. For this case, m was considered to range from -1 to +3. Figure 18 shows the temperature distribution with various power-law indices. When the power-law index (m) increased, the temperature decreased, since the FG sphere got cold faster. Figure 19 shows the variation of radial displacement due to thermal load and magnetic field with various power- law indices. Since an increase in m results in a higher gravity of the sphere, the radial displacement is decreased. Figure 20 shows the variation of radial stress due to thermal load and magnetic field with various power-law indices. As can be observed, the radial stress becomes 0 at the inner radius of the sphere, since there is no constraint
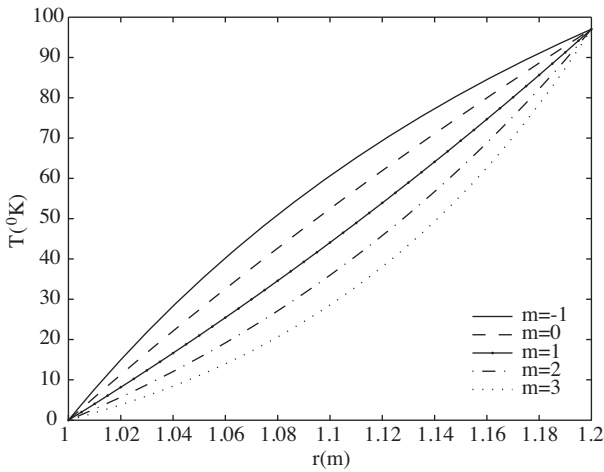

Figure 18. Temperature distribution along the thickness of the FG sphere with various power-law indices at $\theta = \pi/4$ (example 2).
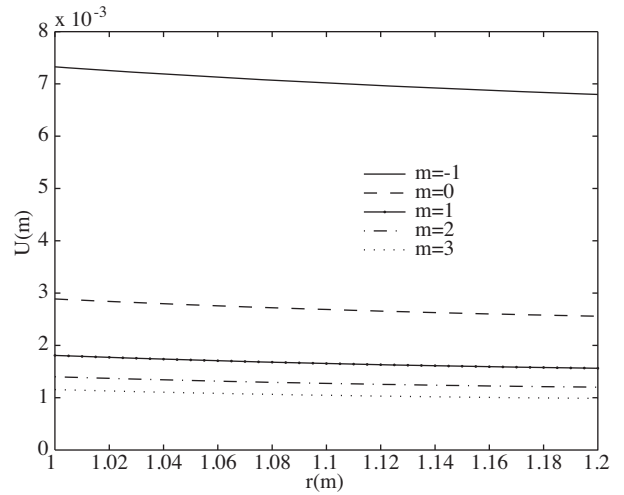

Figure 19. Radial displacement due to thermal load and magnetic field along the thickness of the FG sphere with various power-law indices at $\theta = \pi/4$ (example 2).
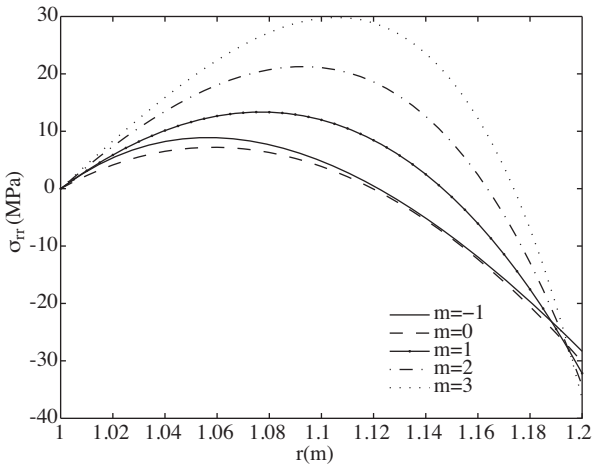

Figure 20. Radial stress due to thermal load and magnetic field along the thickness of the FG sphere with various power-law indices at $\theta = \pi/4$ (example 2).

Figure 21. Circumferential stress due to thermal load and magnetic field along the thickness of the FG sphere with various power-law indices at $\theta = \pi/4$ (example 2).
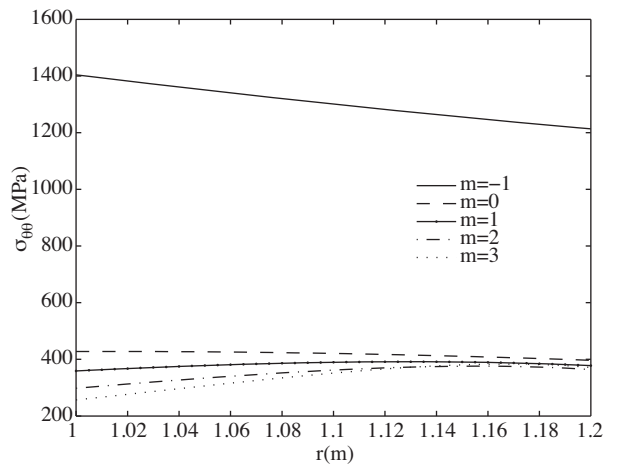
at the inner radius. By increasing the power-law index (m), the radial stress is increased. Figure 21 shows the circumferential stress distribution due to thermal load and magnetic field with various power-law indices. Contrary to the effect on radial stress, the circumferential stress is decreased by increasing m. Figure 22 shows the shear stress distribution due to thermal load and magnetic field with various power-law indices. Similar to the radial stress distribution, as m is increased, the shear stress is also increased. Figure 23 shows the perturbation magnetic field vector due to thermal load with various power-law indices. By increasing m, the perturbation is decreased.
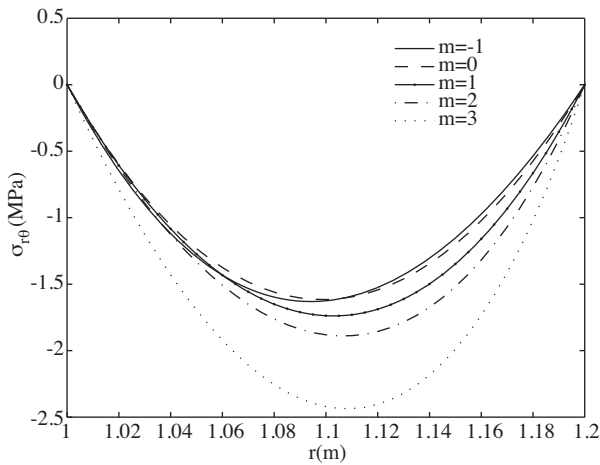

Figure 22. Shear stress due to thermal load and magnetic field along the thickness of the FG sphere with various power-law indices at $\theta = \pi/4$ (example 2).
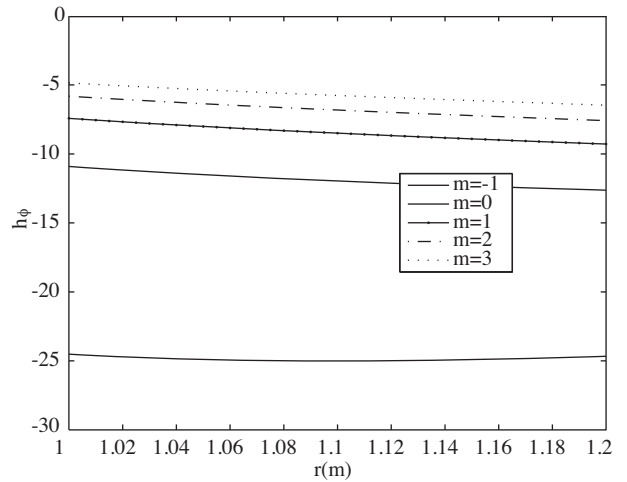

Figure 23. Perturbation of magnetic field vector due to thermal load along the thickness of the FG sphere with various power-law indices at $\theta = \pi/4$ (example 2).

Conclusion

In this paper, the analytical solution for the magneto-thermo-mechanical response of a FG hollow sphere is presented. The analytical solution for stresses and perturbation were determined using the power series method. The material stiffness, thermal expansion coefficient, heat conduction coefficient, and magnetic permeability varied continuously across the thickness direction according to the power-law functions of radial direction. A magnetic field resulted in decreases of the radial displacement and circumferential stress due to mechanical load, and had a negligible effect on mechanical radial stress. The magnetic field also resulted in increases of the radial displacement and the radial and circumferential stresses due to thermal load. By increasing the power-law index (m), the above mentioned quantities, due to mechanical loads, were all decreased. Increasing the power-law indices in the presence of thermal loads resulted in increased radial stress and shear stress values, but had a reverse effect on temperature, radial displacement, circumferential stress, and perturbation of the magnetic field vector distributions. In general, the effect of mechanical loads with a magnetic field was more significant when compared to the effect of thermal loads with a magnetic field.

Acknowledgment

Appendix

$$d_1 = (m_2 + \delta_{1n} + 1)(m_2 + \delta_{1n})(1 + A) + (m_1 + 2 + 2A)(m_2 + \delta_{1n} + 1) + 2(\frac{m_1\nu}{1-\nu} - 1 - A) - n(n+1)(\frac{1-2\nu}{2-2\nu})$$

$$d_2 = n(n+1)[(m_2 + \delta_{1n} + 1)(\frac{1}{2-2\nu} + A) + (\frac{m_1\nu}{1-\nu} - \frac{3-4\nu}{2-2\nu} - A)]$$

$$d_3 = -[(m_2 + \delta_{1n} + 1)(\frac{1}{1-2\nu} + B) + m_1 + \frac{4-4\nu}{1-2\nu} + 2B]$$

$$d_4 = (m_2 + \delta_{1n} + 1)(m_2 + \delta_{1n}) + (m_1 + 2)(m_2 + \delta_{1n} + 1) - n(n+1)(\frac{2-2\nu}{1-2\nu}) - m_1 - Bn(n+1)$$

$$d_5 = \frac{(1+\nu)\alpha_0 a^{-m_2}}{(1-\nu)}(m_1 + m_2 + \delta_{1n})E_{1n}$$

$$d_6 = -\frac{(2+2\nu)\alpha_0 a^{-m_2}}{1-2\nu}E_{1n}$$

$$d_7 = (m_2 + \delta_{2n} + 1)(m_2 + \delta_{2n})(1 + A) + (m_1 + 2 + 2A)(m_2 + \delta_{2n} + 1) + 2(\frac{m_1\nu}{1-\nu} - 1 - A) - n(n+1)(\frac{1-2\nu}{2-2\nu})$$

$$d_8 = n(n+1)[(m_2 + \delta_{2n} + 1)(\frac{1}{2-2\nu} + A) + (\frac{m_1\nu}{1-\nu} - \frac{3-4\nu}{2-2\nu} - A)]$$

$$d_9 = -[(m_2 + \delta_{2n} + 1)(\frac{1}{1-2\nu} + B) + m_1 + \frac{4-4\nu}{1-2\nu} + 2B]$$

$$d_{10} = (m_2 + \delta_{2n} + 1)(m_2 + \delta_{2n}) + (m_1 + 2)(m_2 + \delta_{2n} + 1) - n(n+1)(\frac{2-2\nu}{1-2\nu}) - m_1 - Bn(n+1)$$

$$d_{11} = \frac{(1+\nu)\alpha_0 a^{-m_2}}{(1-\nu)}(m_1 + m_2 + \delta_{2n})E_{2n}$$

$$d_{12} = -\frac{(2+2\nu)\alpha_0 a^{-m_2}}{1-2\nu}E_{2n}$$

$$s_1 = \frac{(1-2\nu)(m_1 + 2 + 2A)(m_1 + \frac{4-4\nu}{1-2\nu} + 2B)}{(1+A)(1+B(1-2\nu))} + 2(\frac{m_1\nu}{(1-\nu)(1+A)} - 1)$$

$$s_2 = \frac{(1+\nu)\alpha_0 a^{-m_2}(m_1 + m_2)}{(1+A)(1-\nu)} - \frac{(m_1 + 2 + 2A)(2+2\nu)\alpha_0 a^{-m_2}}{(1+A)(1+B(1-\nu))}, \quad s_3 = \frac{(1+\nu)\alpha_0 a^{-m_2}}{(1+A)(1-\nu)}$$

Nomenclature

$\vec{U}, u$ radial displacement vector and radial displacement (m)

$\vec{V}, v$ circumferential displacement vector and circumferential displacement (m)

α thermal expansion coefficient $(1/\,^\circ K)$

σ_{ij} components of stresses (N/m^2)

T temperature change $(^\circ K)$

ρ mass density (kg/m^3)

r radial variable (m)

θ circumferential variable (rad)

$\vec{H}$ magnetic intensity vector (A/m)

$\vec{h}$ perturbation of magnetic field vector

$\vec{J}$ electric current density vector

μ magnetic permeability (H/m)

a, b inner and outer radius of the FG hollow sphere (m)

References

Abd-Alla, A.M., Hammad, H.A.H., Abo-Dahab, S.M., "Magneto-Thermo-Viscoelastic Interactions in an Unbounded Body with a Spherical Cavity Subjected to a Periodic Loading", J. Appl. Math & Comp., 155, 235-248, 2004.

Arani, A.G., Salari, M., Khademizadeh, H. and Arefmanes, A., "Magnetothermoelastic Transient Response of a Functionally Graded Thick Hollow Sphere Subjected to Magnetic and Thermoelastic Field", Arch. Appl. Mech., 79, 481-497, 2009.

Chen, W.Q. and Lee, K.Y., "Alternative State Space Formulations for Magnetoelectric Thermoelasticity with Transverse Isotropy and the Application to Bending Analysis of Nonhomogeneous Plates", J. Solids & Structures, 40, 5689-5705, 2003.

Dai, H.L. and Fu, Y.M., "Magnetothermoelastic Interactions in Hollow Structures of Functionally Graded Material Subjected to Mechanical Loads", Intern. J. Pressure Vessels and Piping, 84, 132-138, 2007.

Dai, H.L. and Wang, X., "The Dynamic Response and Perturbation of Magnetic Field Vector of Orthotropic Cylinders Under Various Shock Loads", Intern. J. Pressure Vessels and Piping, 83, 55-62, 2006.

Eslami, M.R., Babai, M.H. and Poultangari, R., "Thermal and Mechanical Stresses in a Functionally Graded Thick Sphere", Intern. J. Pressure Vessel and Piping, 82, 522-527, 2005.

Genç, M.S., Özışık, G. and Yapıcı, H., "A Numerical Study of the Thermally Induced Stress Distribution in a Rotating Hollow Disk Heated by a Moving Heat Source Acting on One of the Side Surfaces", Proc IMechE, Part C - J. Mech. Eng. Sci., 223, 1877-1887, 2009.

Lee, Z.Y., "Magnetothermoelastic Analysis of Multilayered Conical Shells Subjected to Magnetic and Vapor Fields", Intern. J. Thermal Sciences, 48, 50-72, 2009.

Loghman, A., Arani, A.G., Amir, S. and Vajedi, A., "Magnetothermoelastic Creep Analysis of Functionally Graded Cylinders", Int. J. Pressure Vessels and Piping, 87, 389-395, 2010.

Lutz, M.P. and Zimmerman, R.W., "Thermal Stresses and Effective Thermal Expansion Coefficient of a Functionally Gradient Sphere", J. Thermal Stresses, 19, 39-54, 1996.

Mahdi, M. and Zhang, L., "Applied Mechanics in Grinding. V. Thermal Residual Stresses", Int. J. Mach. Tools Manuf., 37, 619-633, 1997.

Maruszewski, B., "Dynamical Magnetothermoelastic Problem in Circular Cylinders - I: Basic Equations", Intern. J. Engineering Science, 19, 1233-1240, 1981.

Massalas, C.V., "A Note on Magnetothermoelastic Interactions", Intern. J. Engineering Science, 29, 1217-1229, 1991.

Misra, J.C., Samanta, S.C., Chakrabarti, A.K. and Misra, S.C., "Magnetothermoelastic Interaction in an Infinite Elastic Continuum with a Cylindrical Hole Subjected to Ramp-Type Heating", Intern. J. Engineering Science, 29, 1505-1514, 1991.

Misra, S.C., Samanta, S.C. and Chakrabarti, A.K., "Transient Magnetothermoelastic Waves in a Viscoelastic Half-Space Produced By Ramp-Type Heating Of Its Surface", J. Computers & Structures, 43, 951-957, 1992.

Moulik, P.N., Yang, H.T.Y. and Chandrasekar, S., "Simulation of Thermal Stresses Due to Grinding", Int. J. Mech. Sci., 43, 831-851, 2001.

Özışık, G. and Genç, M.S, "Temperature and Thermal Stress Distribution in a Plate Heated From One Side Surface with a Moving Heat Source", J. Faculty of Engineering and Architecture of Gazi University, 23, 601-610, 2008.

Özışık, M.N., "Heat Conduction", Wiley & Sons, 1980.

Paul, H.S. and Narasimhan, R., "Magnetothermoelastic Stress Waves in a Circular Cylinder", Intern. J. Engineering Science, 25, 413-425, 1987.

Poultangari, R., Jabbari, M. and Eslami, M.R., "Functionally Graded Hollow Spheres under Non-Axisymmetric Thermo-Mechanical Loads", Int. J. Pressure Vessels and Piping 85, 295-305, 2008.

Sen, S., Aksakal, B., and Ozel, A., "Transient and Residual Thermal Stresses in Quenched Cylindrical Bodies", Int. J. Mech. Sci., 42, 2013-2029, 2000.

Sharma, J.N. and Pal, M., "Rayleigh-Lamb Waves in Magnetothermoelastic Homogeneous Isotropic Plate", Intern. J. Engineering Science, 42, 137-155, 2004.

Tanigawa, Y., Morishita, H. and Ogaki, S., "Derivation of Systems of Fundamental Equations for a Three-Dimensional Thermoelastic Field With Nonhomogeneous Material Properties and its Application to a Semi-Infinite Body", J. Thermal Stresses, 22, 689-711, 1999.

Tianhu, H., Xiaogeng, T. and Yapeng, S., "A Generalized Electromagneto-Thermoelastic Problem for an Infinitely Long Solid Cylinder", Euro. J. Mech. A/Solids, 24, 349-359, 2005.

Tianhu, H., Yapeng, S. and Xiaogeng, T., "A Two-Dimensional Generalized Thermal Shock Problem for a Half-Space in Electromagneto-Thermoelasticity", Intern. J. Engineering Science, 42, 809-823, 2004.

Wang, H.M. and Dink, H.J., "Transient Responses of a Magneto-Electro-Elastic Hollow Sphere for Fully Coupled Spherically Symmetric Problem", Euro. J. Mech. A/Solids, 25, 965-980, 2006.

Wang, X. and Dong, K., "Magnetothermodynamic Stress and Perturbation of Magnetic Field Vector in a Non-Homogeneous Thermoelastic Cylinder", Euro. J. Mech. A/Solids, 25, 98-109, 2006.

Yapıcı, H. and Baştürk, G., "Reduction of Thermally Induced Stress in a Solid Disk Heated with Radially Periodic Expanding and Contracting Ring Heat Flux", J. Mater. Process. Tech., 180, 279-290, 2006.

Yapıcı, H., Genç, M.S., and Özışık, G., "Transient Temperature and Thermal Stress Distributions in a Hollow Disk Subjected to a Moving Uniform Heat Source", J. Therm. Stress, 31, 476-493, 2008.

Yapıcı, H., Özışık, G. and Genç, M.S., "Non-Uniform Temperature Gradients and Thermal Stresses Produced by a Moving Heat Flux Applied on a Hollow Sphere", SADHANA-Academy Proc. Eng. Sci., 35, 195-213, 2010.